Highly dispersed Cd cluster supported on TiO2 as an efficient catalyst for CO2 hydrogenation to methanol

Wang, J.; Meeprasert, J.; Han, Z.; Wang, H.; Feng, Z.; Tang, C.; Sha, F.; Tang, S.; Pidko, E.A.; More Authors

Publication date
2022

Document Version
Accepted author manuscript

Published in
Chinese Journal of Catalysis

Highly dispersed Cd cluster supported on TiO_2 as an efficient catalyst for CO_2 hydrogenation to methanol

Jijie Wang [a†], Jittima Meeprasert [b†], Zhe Han [c,a†], Huan Wang [a], Zhendong Feng [a, d], Chizhou Tang [a, d], Feng Sha [c,a], Shan Tang [a, d], Guanna Li [e, f], Evgeny A. Pidko [b,*], Can Li [a,*]

[a] State Key Laboratory of Catalysis, Dalian Institute of Chemical Physics, Chinese Academy of Sciences, Dalian, 116023, China.

[b] Inorganic Systems Engineering, Department of Chemical Engineering, Delft University of Technology, Van der Maasweg 9, 2629 HZ Delft, the Netherlands.

[c] School of Materials Science and Engineering & National Institute for Advanced Materials, Nankai University, Tianjin, 300350, China.

[d]University of Chinese Academy of Sciences, Beijing 100049, China.

[e] Biobased Chemistry and Technology, Wageningen University & Research, the Netherlands.

[f] Laboratory of Organic Chemistry, Wageningen University & Research, the Netherlands.

† These authors contributed equally to this work.

* Corresponding author. E-mail: canli@dicp.ac.cn

E.A.Pidko@tudelft.nl

Abstract: The conversion of CO_2 with high activity and high selectivity to methanol remains challenging because of both the kinetics and thermodynamics difficulties associated with the chemical reactivity of CO_2. Herein, we report a new catalyst of Cd/TiO_2 enabling 81% methanol selectivity at 15.8% CO_2 conversion with the CH_4 selectivity below 0.7%. The combination of experimental and computational studies show that the unique electronic properties of Cd cluster supported on TiO_2 are responsible for the high selectivity for CO_2 hydrogenation to methanol via a HCOO* pathway realized at the interface catalytic sites.

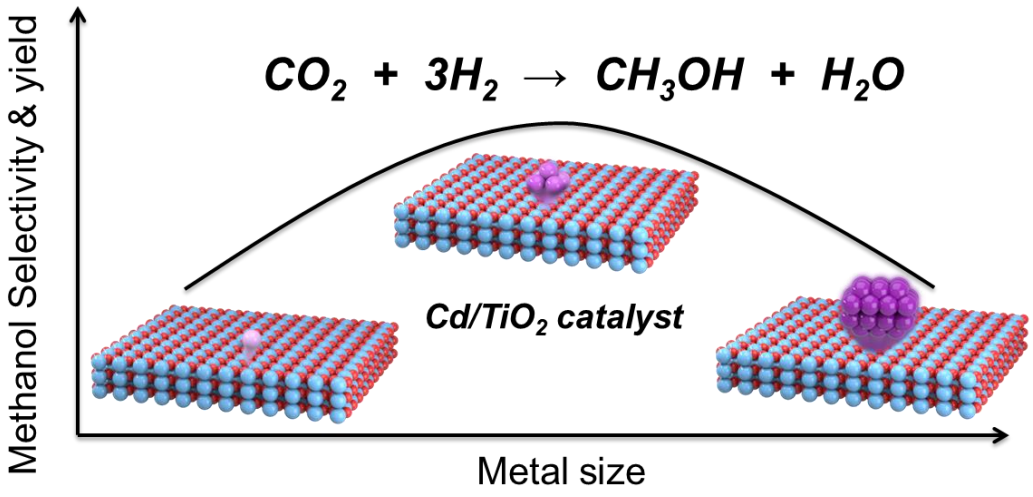

1. Introduction

Carbon dioxide capture and utilization (CCU) using renewable energy is an effective way to achieve carbon neutrality, thus drawing increasing attention from industry and academia worldwide. A promising route for CO_2 utilization is methanol production ($CO_2 + 3H_2 \rightarrow CH_3OH + H_2O$) since methanol can be used as an easily transportable fuel, an H_2-storage molecule, or a precursor for the production of olefins and aromatics [1-2].

Heterogeneous catalysts are commonly available for CO_2 hydrogenation to methanol by using a fixed bed reactor, which is capable for scale-up industrial applications [3-7]. Until now, CuZnO catalysts have been widely investigated for CO_2 hydrogenation to methanol [8-15]. However, the methanol selectivity reported so far hardly exceeds 60% under the optimal operation conditions because of the competing side reactions, such as reverse water-gas shift reaction (RWGS) [16]. Besides, Cu-based catalysts usually suffer from deactivation caused by sintering [17]. Thus, non-Cu catalysts have drawn increasing attentions in recent years [18]. For instance, MnO_x/m-Co_3O_4 [19], Co@SiO_2 [20], and MoS_2 [21] were reported to be able to selectively hydrogenate CO_2 to methanol. Unfortunately, these catalysts produce up to 2-10% CH_4 in course of the reaction, far from meeting the industrial requirement. High selectivity to methanol has been achieved using In_2O_3/ZrO_2 [16, 22-24] and MO_xZrO_2

(M=Zn, Cd, Ga) solid solutions catalysts [25, 26] with the trade off of the low CO_2 conversion. NiGa and PdGa alloys catalysts also show excellent activity, however, only under atmospheric pressure [27-28]. It seems to be a general trend that better performance can be achieved when the catalyst contains two components, of which one is a metal oxide (ZnO, ZrO_2) responsible for CO_2 activation, and the other is a metal or a reducible metal oxide (Cu, ZnO_x, In_2O_x, Ga_2O_x, MnO_x) for H_2 activation. These observations inspired us to explore other materials possessing the similar property. In this work, we found that a Cd cluster based Cd/TiO_2 catalyst shows 81% methanol selectivity at CO_2 conversion of 15.8%, while enabling to keep the CH_4 under 0.7% at 5 MPa. The TOF of methanol formation for Cd/TiO_2 catalyst is 43 $mol \cdot mol_{active\ metal}^{-1} \cdot h^{-1}$ at 2 MPa, 290 ^oC and 24000 $ml \cdot g_{cat}^{-1} \cdot h^{-1}$, which is 26 times of that for CuZnO catalyst and 4 times of that for $ZnO\text{-}ZrO_2$ catalyst under their respective optimized conditions. Further experimental study and DFT calculations indicate that the interface between Cd cluster and TiO_2 are the active center for the hydrogenation of CO_2 to methanol, rather than isolated Cd site or Cd nanoparticle supported on TiO_2.

2. Experimental

2.1 Catalyst preparation

TiO_2 was prepared by hydrolysis method using $TiO(C_4H_9)_4$. The obtained suspension was filtered, washed, and calcined at 500 ^oC in static

air for 3 h. If the TiO_2 was treated with H_2 at 500 °C for 2 h, TiO_2(D) would be got. A series of x% Cd/TiO_2 catalysts (x% represents molar percentage of Cd, metal base) were prepared by wet impregnation using $Cd(NO_3)_2 \cdot 4H_2O$ as precursor. When the TiO_2(D) was used as support for Cd/TiO_2 catalyst, the sample was labled with Cd/TiO_2(D). The Cd/TiO_2 catalyst were also prepared by precipitaion method and physical mixed method, which labled with Cd/TiO_2(P) and Cd/TiO_2(M), respectively. CuZnO and ZnO-ZrO_2 catalysts were prepared by precipitation method. The Cu content in CuZnO catalyst is 70% (optimized content). The ZnO content in ZnO-ZrO_2 catalyst is 13% (optimized content).

2.2 Catalyst evaluation

The activity tests of the catalysts for CO_2 hydrogenation to methanol were carried out in a tubular fixed-bed continuous-flow reactor equipped with gas chromatography (GC). All catalysts were pressed, crushed, and sieved to the size of 40–80 mesh for the activity evaluation. Before the reaction, the catalyst (0.1 g, diluted with 0.4 g quartz sand) was pretreated in a H_2 or N_2 stream (0.1 MPa and 20 mL/min) at given temperatures. The reaction was conducted under reaction conditions of 2.0～5.0 MPa, 200～400 °C, $V(H_2)/V(CO_2)/V(Ar)$ = 72/24/4, and GHSV = 6000～24000 mL/(g h). The exit gas from the reactor was maintained at 150 °C and immediately transported to the sampling valve of the GC (Agilent

GC-7890B), which was equipped with thermal conductivity and flame ionization detectors. Propark N and 5A molecular sieves packed columns (2 m×1/8 inch, Agilent) were connected to TCD while TG-BOND-Q capillary columns were connected to FID. The packed column were used for the analysis of CO_2, Ar, CO, and the capillary column (30 m×0.32 mm×10 μm, ThermoFisher) for hydrocarbons, alcohols, and other C-containing products. CO_2 conversion (denoted as X(CO_2)) and the carbon-based selectivity (denoted as S(product)) for the carbon-containing products, including methane, methanol, and dimethyl ether, were calculated with an internal normalization method. Space time yield of methanol was denoted as STY(CH_3OH). All data were collected in 3 h after the reaction started (unless otherwise specified).

Calculation of X(CO_2), S(CH_3OH), S(CO), STY(CH_3OH):

$$X(CO_2)=\frac{f_{CO}A_{CO}+i(f_{CH_4}A_{CH_4}+f_{CH_3OH}A_{CH_3OH}+2f_{CH_3OCH_3}A_{CH_3OCH_3})}{f_{CO_2}A_{CO_2}+f_{CO}A_{CO}+i(f_{CH_4}A_{CH_4}+f_{CH_3OH}A_{CH_3OH}+2f_{CH_3OCH_3}A_{CH_3OCH_3})}$$

$$i=\frac{f_{CH_4-TCD}A_{CH_4-TCD}}{f_{CH_4-FID}A_{CH_4-FID}}$$

$$S(CH_3OH)=\frac{if_{CH_3OH}A_{CH_3OH}}{f_{CO}A_{CO}+i(f_{CH_4}A_{CH_4}+f_{CH_3OH}A_{CH_3OH}+2f_{CH_3OCH_3}A_{CH_3OCH_3})}$$

$$S(CO)=\frac{f_{CO}A_{CO}}{f_{CO}A_{CO}+i(f_{CH_4}A_{CH_4}+f_{CH_3OH}A_{CH_3OH}+2f_{CH_3OCH_3}A_{CH_3OCH_3})}$$

$$STY(CH_3OH)=\frac{GHSV}{22.4}\times V\%(CO_2)\times X(CO_2)\times S(CH_3OH)\times M_{CH_3OH}$$

2.3 Catalyst characterization

The XRD results were collected on a Philips PW1050/81 diffractometer operating in Bragg-Brentano focusing geometry and using CuKα radiation (λ = 1.5418 Å) from a generator operating at 40 kV and 30 mA. SEM images were obtained with JEOL JSM-7800F. HRTEM images were obtained with an JEM-2100 microscope, 200 kV. The samples were prepared by placing a drop of nanoparticle ethanol suspension onto a lacey support film and allowing the solvent to evaporate. STEM were obtained with JEM-ARM200F microscope. The samples were prepared by placing a drop of nanoparticle ethanol suspension onto a lacey support film and allowing the solvent to evaporate. XPS was performed using a Thermo ESCALAB 250Xi with Al K radiation (15 kV, 10.8 mA, hν = 1486.6 eV) under ultrahigh vacuum (5×10^{-7} Pa), calibrated internally by the carbon deposit C(1s) (E_b = 284.6 eV). There is a sample cell that feed gas of CO_2 and H_2 can be induced into and can be heated at the same time. Cd/TiO_2 catalysts were treated with CO_2/H_2=1/3 mixed gas for 2 h under the reaction conditions of 290 ºC, 0.1MPa, then cooled in Ar atmosphere and to be used the XPS measure. EXAFS fitting was performed using VIPER program.The fit was performed alternatively in k and R spaces. When in the R space, it was done in the (Im + Module) mode, mathematically equivalent to the k-fit. The Fourier transformed (FT) data in R space were analyzed by applying CdO and metallic Cd model for Cd−O and Cd−Cd contributions.

A Brook A200 was used for recording EPR spectra at liquid nitrogen temperature. The sample was treated with the feed gas of CO_2 and H_2 (CO_2/H_2=1/3) at 290 ºC, 0.1MPa, then cooled to room temperature keeping the atmosphere of feed gas. In-situ DRIFTS experiments were performed using a FT-IR spectrometer (Bruker, Vertex 70) equipped with a MCT detector. All the DRIFTS experiments are conducted under 0.1MPa. Before measurement, the catalyst was treated with H_2 at 290℃ for 1 h, and then purged with Ar at 290℃. The background spectrum was obtained at 290℃ in Ar flow. Then, the sample was exposed to CO_2 or a CO_2/H_2 mixture consecutively. The in-situ DRIFT spectra were recorded by collecting 64 scans at 4 cm^{-1} resolution.

2.4 DFT calculation

All DFT calculations have been performed using the Vienna Ab Initio Simulation Package (VASP). The generalized gradient approximation (GGA) with PBE exchange and correlation functional was used to account for the exchange-correlation energy. The kinetic energy cutoff of the plane wave basis set was set to 400 eV. The threshold for energy convergence for each iteration was set to 10^{-5} eV. Geometries were assumed to be converged when forces on each atom were less than 0.05 eV/Å. Gaussian smearing of the population of partial occupancies with a width of 0.10 eV was used during iterative diagonalization of the Kohn-Sham Hamiltonian. The bulky TiO_2 unit cell in the phase of anatase was firstly fully optimized.

The optimized lattice vectors of TiO_2 are a = b = 3.799 Å and c = 9.716 Å and $\alpha = \beta = \gamma = 90.00^o$, which have a good agreement with the experiment parameters. For Cd_4/TiO_2 model, 2x4 supercells of anatase TiO_2 (101) surface with a vacuum space of 15 Å were built for investigation of the reaction mechanism. This slab model contains six titanium layers with the bottom three layers were fixed while the rest was allowed to relax during the geometry optimization. The lattice parameters were fixed throughout the surface calculations. For the $CdTiO_3$ model, the optimized lattice vectors of rhombohedral $CdTiO_3$ are a = b = c = 5.893 Å and $\alpha = \beta = \gamma = 53.55^o$.[5] The 1x3 supercell of $CdTiO_3$ (104) surface with a vacuum space of 15 Å were built for the reaction mechanism study. The optimized structure of Cd_4/TiO_2 and $CdTiO_3$ catalysts are shown in Figure S11. The nudged-elastic band method with the improved tangent estimate (CI-NEB) was used to determine the minimum energy path and to locate the transition state structure for each elementary reaction step.

3. Results and Discussion

Cd/TiO_2 catalysts were prepared by wet impregnation using TiO_2 support. The performance of the catalysts for CO_2 hydrogenation was evaluated in the fixed-bed reactor. CH_3OH and CO are the main products detected by GC. Fig. 1(a) summarizes the CO_2 conversion and methanol selectivity for TiO_2-based and Cd-based catalysts. For Cd/TiO_2 catalyst, methanol selectivity of 71% can be obtained when CO_2 conversion

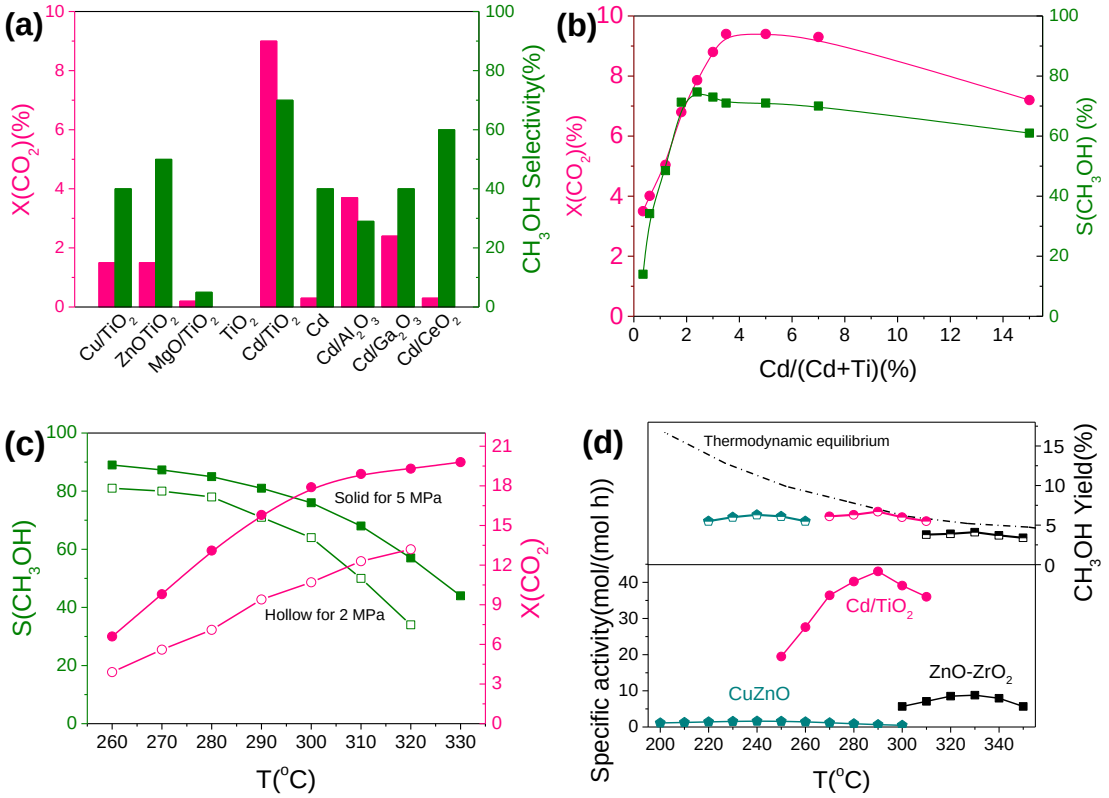

Fig. 1 Catalytic performance. **(a)** CO_2 conversion and methanol selectivity for different catalysts. (**b)** Dependence of catalytic performance on the Cd/(Cd+Ti) molar ratio. (**c**) Variation of CO_2 conversion and methanol selectivity of 3.5%Cd/TiO_2 under different pressures and temperatures. (**d**) Methanol yield and specific activity for CuZnO, Cd/TiO_2, and ZnO-ZrO_2 catalysts at different temperatures. Standard reaction conditions: 2.0 MPa, H_2/CO_2 = 3/1, 290 ℃, GHSV = 24000 mL·g_{cat}^{-1}·h^{-1}.

reaches 9.4% under 2 MPa, 290 ℃, CO_2/H_2 = 1:3, 24000 mL·g_{cat}^{-1}·h^{-1}. In contrast, no methanol was detected for TiO_2, and methanol selectivity of 40% was obtained using Cd along, however, only 0.3% of CO_2 was converted. Other composite catalysts such as Cd/Al_2O_3, Cd/CeO_2, Cd/Ga_2O_3, Cu/TiO_2, ZnO/TiO_2, and MgO/TiO_2 all exhibit low methanol

selectivity (≤ 50%) and CO_2 conversion (≤ 4%). These data suggest the unique reactivity of Cd/TiO_2 catalyst for CO_2 hydrogenation to methanol. Fig. 1(b) shows the relationship between the catalytic performance and the Cd loading (Cd/(Cd+Ti) molar ratio). For the 0.35-3.5%Cd/TiO_2, both the activity and selectivity increase with the increase of Cd loading and reach the maximum at 3.5%Cd. Further increasing the Cd loading from 3.5% to 7% results in a slight decrease of both activity and selectivity. Fig. 1(c) shows the effect of temperature and pressure on the performance of 3.5%Cd/TiO_2 catalyst. It can be seen that CO_2 conversion increases with the increase of temperature but the methanol selectivity decrease, while higher pressure is favorable for both CO_2 conversion and methanol selectivity. When the pressure increased to 5 MPa, 3.5%Cd/TiO_2 catalyst exhibits 81% methanol selectivity and 15.8% CO_2 conversion. At the same time, the selectivity of dimethyl ether and methane is below 1% and 0.7%, respectively. Fig. 1(d) shows the methanol yield and specific activity (defined as methanol yield per active metal per hour) for Cd/TiO_2, CuZnO, and ZnO-ZrO_2. The mole-specific activity for Cd/TiO_2 catalyst is 43 $mol \cdot mol_{active\ metal}^{-1} \cdot h^{-1}$, 26 times that for CuZnO catalyst, and 4 times that for ZnO-ZrO_2 catalyst (Table S1-2). 3.5%Cd/TiO_2 catalyst exhibits a methanol yield of 6.7% ($X(CO_2)$=9.4%, $S(CH_3OH)$=71%), which is approaching the thermodynamic equilibrium under the conditions of 2 MPa, 290 ^oC.

Fig. 2(a) shows the X-Ray diffraction (XRD) of fresh Cd/TiO_2 catalysts. All the diffraction peaks are attributed to TiO_2 when the Cd loading is below 3.5%. Diffraction peaks due to $CdTiO_3$ appear only when Cd loading exceeds 5%. It indicates that the Cd species are highly dispersed on the surface of TiO_2 at low Cd loadings and gradually aggregates to nanoparticles when the Cd loading exceeds 5%. Fig. 2(b-c) show the XRD spectra of the used catalysts. It can be seen that part of $CdTiO_3$ starts to be reduced to metallic Cd when the Cd loading exceeds 5%. There is no obvious signal of Cd species in the XRD spectra when the Cd loading is below 3.5%. The scanning electron microscopy (SEM) image of the used 3.5% Cd/TiO_2 catalyst shows that the sample is mainly in small spheres, of which the size is approximately 10-20 nm (Fig. S1a). The interplanar spacing of the used 3.5% Cd/TiO_2 catalyst is ca. 0.35 nm, which is attributed to the (101) face space of anatase TiO_2. Element distribution analysis indicates that these Cd species are distributed homogeneously on the surface of TiO_2 (Fig. S1). The catalyst structure was further characterized by aberration-corrected scanning transmission electron microscopy with high angle circular dark field image (STEM). Fig. 2(d) shows Cd species of used 0.35%Cd/TiO_2 catalyst are atomically dispersed with isolated Cd sites on TiO_2. For used 3.5%Cd/TiO_2 catalyst, a lot of sub-nanometer Cd clusters emerge besides isolated Cd site (Fig. 2(e)). When the Cd loading further increases to 7%, nanometre-size Cd

particles are observed in addition to Cd clusters and isolated Cd sites (Fig. 2(f)). The bigger Cd particles are confirmed by the SEM in the backscatter

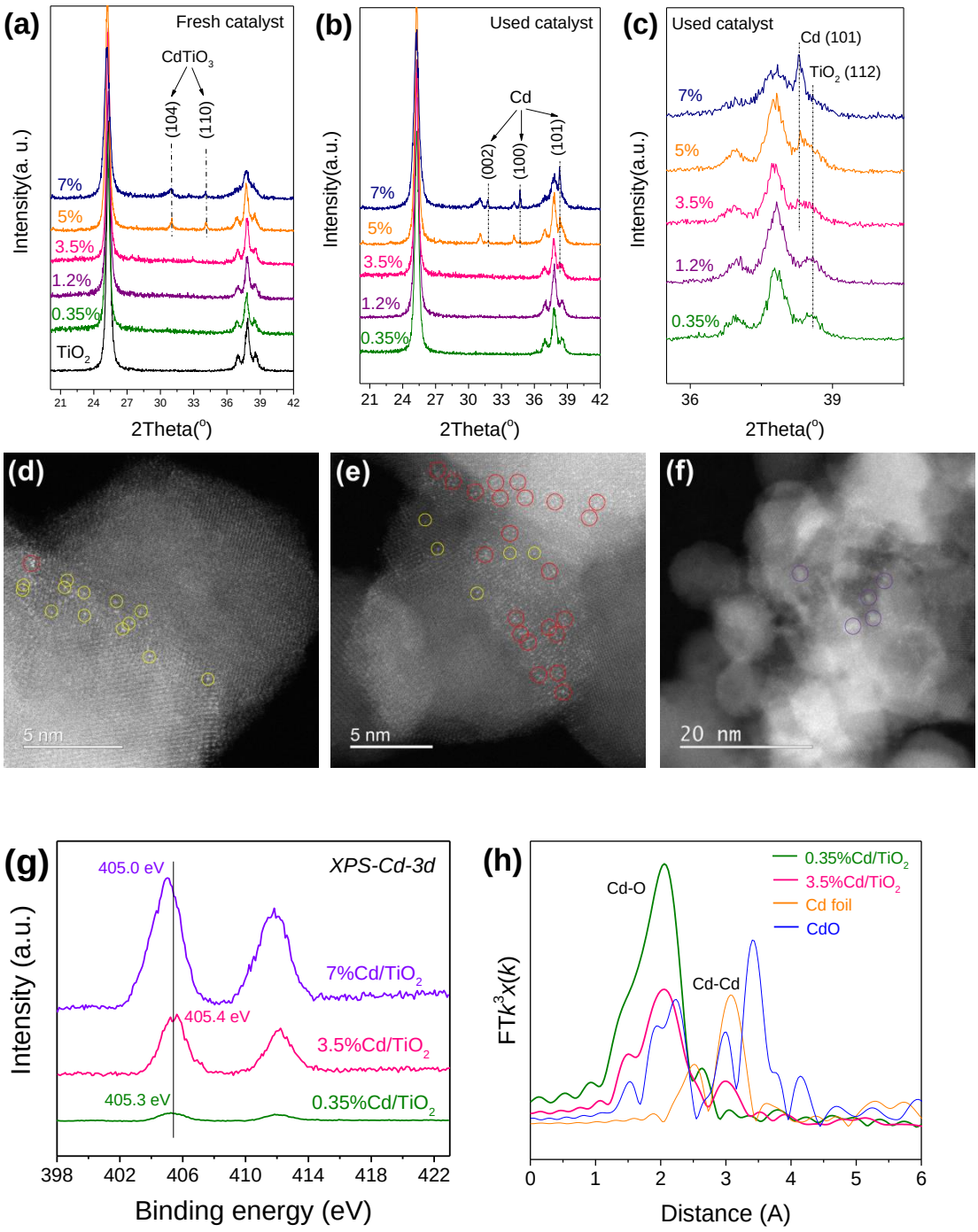

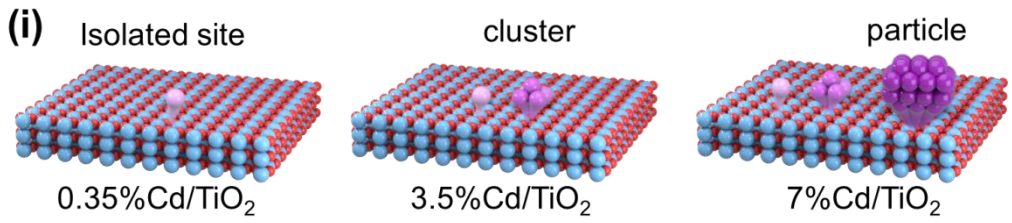

Fig. 2 Structural characterization. **(a)** XRD patterns of fresh Cd/TiO_2 catalysts. (**b-c)** XRD patterns of used Cd/TiO_2 catalysts. (**d-f)** Aberration-corrected STEM-HAADF image of $0.35\%Cd/TiO_2$ (**d**), $3.5\%Cd/TiO_2$ (**e**), and $7\%Cd/TiO_2$ (**f**), The ones in the yellow circle are isolated Cd sites, The ones in the red circle are Cd clusters, The ones in the purple circle are Cd particles. (**g)** XPS of Cd/TiO_2 catalysts treated by CO_2/H_2 mixed gas. (h**)** EXAFS spectra with k^3-weighted data of $0.35\%Cd/TiO_2$ and $3.5\%Cd/TiO_2$. (**i)** Schematic structure illustration of Cd/TiO_2 catalysts.

electron imaging mode for $7\%Cd/TiO_2$ (Fig. S2), which is in line with the XRD results. The electronic property of the Cd/TiO_2 catalysts treated by CO_2/H_2 mixed gas under the reaction temperature were studied by X-ray photoelectron spectroscopy (Fig. 2(g)). The Cd $3d_{5/2}$ peak of $0.35\%Cd/TiO_2$ and 3.5% Cd/TiO_2 locate at 405.3 eV and 405.4 eV, respectively, implying that the Cd is in the +2 oxidation state [29]. It may because of the strong interaction among Cd, O and Ti. The Cd $3d_{5/2}$ peak of $7\%Cd/TiO_2$ locates at 405.0 eV, which represent the the binding energy of Zero-valent Cd [29], indicating that Cd species is reduced to metal during the reaction. Fig. 2(h) shows the results of extended X-ray absorption fine structure (EXAFS) for used $0.35\%Cd/TiO_2$ and $3.5\%Cd/TiO_2$. For the 0.35% Cd/TiO_2 sample, a strong peak at ca. 2 Å

with a CN of 5.7 was identified for the first Cd−O shell, which is attributed to the scattering between the Cd center and its surrounding oxygen atoms in single nuclear Cd species. For the 3.5% Cd/TiO_2 sample, besides the first Cd−O shell with a CN of 3.0, the second Cd-Cd shell with a CN of 1.3 is also observed at ca. 3.0 Å (Fig. S3, Table S3). It indicates that the Cd center is linked to both O atom and Cd atom, however, the intensity of Cd-O is higher than that of Cd-Cd. Based on these characterization results, a model structure of the Cd/TiO_2 catalyst is schematically depicted in Fig. 2(i).

Correlating the catalytic performance with structure of 3.5%Cd/TiO_2 catalyst, it is not difficult to find that sub-nanometer Cd species play an important role in CO_2 hydrogenation to methanol. 7%Cd/TiO_2 has an additional Cd nanoparticle contrasted with the structure of 3.5%Cd/TiO_2, however, both show similar catalytic performances, suggesting that Cd nanoparticle has a minor contribution to the reactivity. The negligible reactivity is also observed for Cd catalyst alone. Cd/TiO_2 catalysts were also prepared by precipitation and physical mixing methods, labeled as Cd-TiO_2(P) and Cd/TiO_2(M), respectively. The structural characterizations of these two catalysts show that isolated Cd site and Cd cluster are present on the TiO_2 surface (Fig. S4-5). Interestingly, all the catalysts show similar catalytic performances after optimizing the Cd content and the calcination temperature (Table S4). It is found that the

0.35%Cd/TiO_2 catalyst, which has a uniform distribution of isolated Cd site supported on TiO_2, only has a methanol selectivity of 13%. In contrast, the 3.5%Cd/TiO_2 catalyst, which has a mixed structure of isolated Cd site and Cd cluster supported on TiO_2, has a methanol selectivity of 71%. In addition, 3.5%Cd/TiO_2 catalyst has a lower apparent activation barrier (E_a) of 63.1 kJ/mol than that of 0.35%Cd/TiO_2 (E_a = 88.6 kJ/mol) for CO_2 hydrogenation to methanol (Fig. S6). It is thus proposed that the Cd cluster interacted with TiO_2 is probably the true active center for CO_2 hydrogenation to methanol.

Oxygen vacancy (O_v) always plays an important role in TiO_2-based catalyst [30]. To prove this point, electron paramagnetic resonance (EPR) was used to investigate the effect of O_v on the catalytic performance of Cd/TiO_2 catalyst. The results show that the amount of oxygen vacancy decreased with the increase of Cd loading for Cd/TiO_2 catalyst. Considering that the catalytic performance of 3.5%Cd/TiO_2 is much better than that of 0.35%Cd/TiO_2, it is speculated that O_v is not a key factor accounting for the high catalytic activity of Cd/TiO_2 catalyst. This point can also be verified by the fact that the Cd/TiO_2(D), which was prepared by impregnating Cd on the TiO_2 contains a lot of O_v (Fig. S7), shows similar catalytic performance to that of Cd/TiO_2 (Table S4).

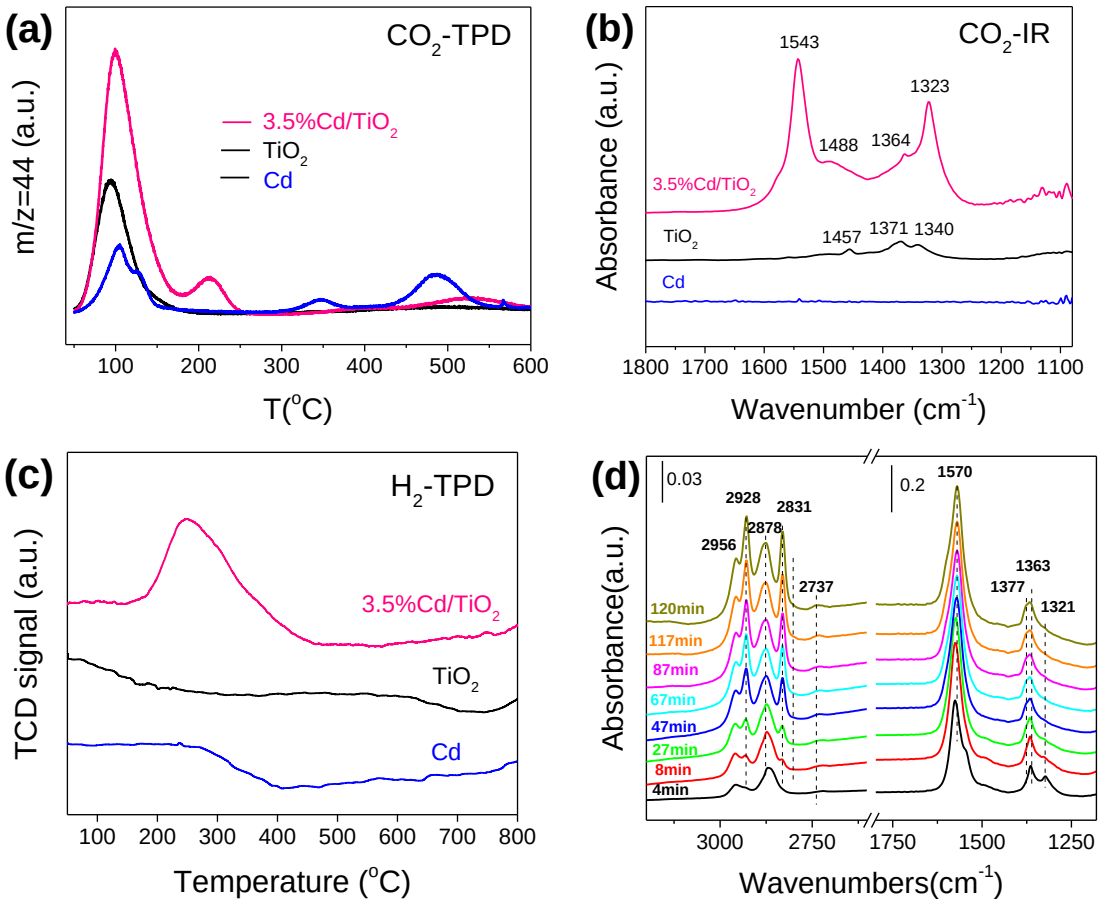

Fig. 3 Surface reactivity. **(a)** CO_2-TPD of 3.5%Cd/TiO_2, TiO_2 and Cd. (**b)** In-situ DRIFT spectra of surface species formed from CO_2 adsorption. (**c)** H_2-TPD of 3.5%Cd/TiO_2, TiO_2 and Cd. (**d)** In-situ DRIFT spectra of surface species formed during the reaction for 3.5%Cd/TiO_2.

CO_2 and H_2 adsorption-desorption experiments were carried out for Cd/TiO_2, TiO_2 and Cd. Fig. 3(a) shows the total CO_2 adsorption amounts for Cd/TiO_2 are much higher than that for TiO_2 and Cd, especially under 300°C. Fig. 3(b) shows the in-situ IR spectra of Cd/TiO_2, TiO_2 and Cd recorded at 290°C after the exposure to CO_2. Four peaks are observed at 1323, 1364, 1488, and 1543 cm^{-1} for Cd/TiO_2. The peaks at 1323, 1364, and 1543 cm^{-1} are attributed to the carboxylate (CO_3^{2-}) species, while the peak at 1488 cm^{-1} is attributed to the bicarbonate (HCO_3^-) species [31]. A

small amount of CO_3^{2-} species was observed for TiO_2 and there are almost no CO_2 adsorption species over Cd. According to the results of CO_2-TPD and CO_2-IR, it is deduced that there is a new site that affords CO_2 adsorption for Cd/TiO_2 compared with TiO_2 and Cd. Fig. 3(c) shows the H_2-TPD results of Cd/TiO_2, TiO_2 and Cd. It can be seen that Cd/TiO_2 exhibits a much higher H_2 adsorption capability than TiO_2 and Cd, indicating there is also a new site for H_2 adsorption. Based on the results of CO_2/H_2 adsorption-desorption experiments and structure characterization, it is concluded that Cd cluster interacted with the surface O-Ti moieties of TiO_2 is the active center for CO_2 and H_2 adsorption. Furthermore, the effect of CO_2 and H_2 concentration on the reaction rate was investigated as well. The results show an approximately 1.8 order dependence on the H_2 partial pressure, while the CO_2 reaction order is 0.6. This indicates that H_2 adsorption has a more significant contribution than CO_2 to the reaction rate (Fig. S8).

To further understand the reaction mechanism on Cd/TiO_2 catalyst, the surface species evolved in the CO_2 hydrogenation reaction were monitored by in-situ diffuse reflectance infrared Fourier transform spectroscopy (DRIFTS). Fig. 3(d) shows the infrared vibration peaks of intermediate species when 3.5%Cd/TiO_2 is exposed to CO_2/H_2 gas at 290°C. The peaks at 1363, 1377, 1570, 2737, 2878 and 2956 cm^{-1} are assigned to the formate ($HCOO^-$) species. The peaks at 2831 and 2928

cm^{-1} are attributed to the H_3CO^* species [13] (Table S5). After changing the gas from CO_2/H_2 to N_2 at 290℃, the peaks belong to $HCOO^*$ and H_3CO^* species almost disappear, indicating that the $HCOO^*$ is probably the active intermediate formed during CO_2 hydrogenation to methanol. The result of C1s-XPS is in line with the results of in-situ IR (Fig. S9).

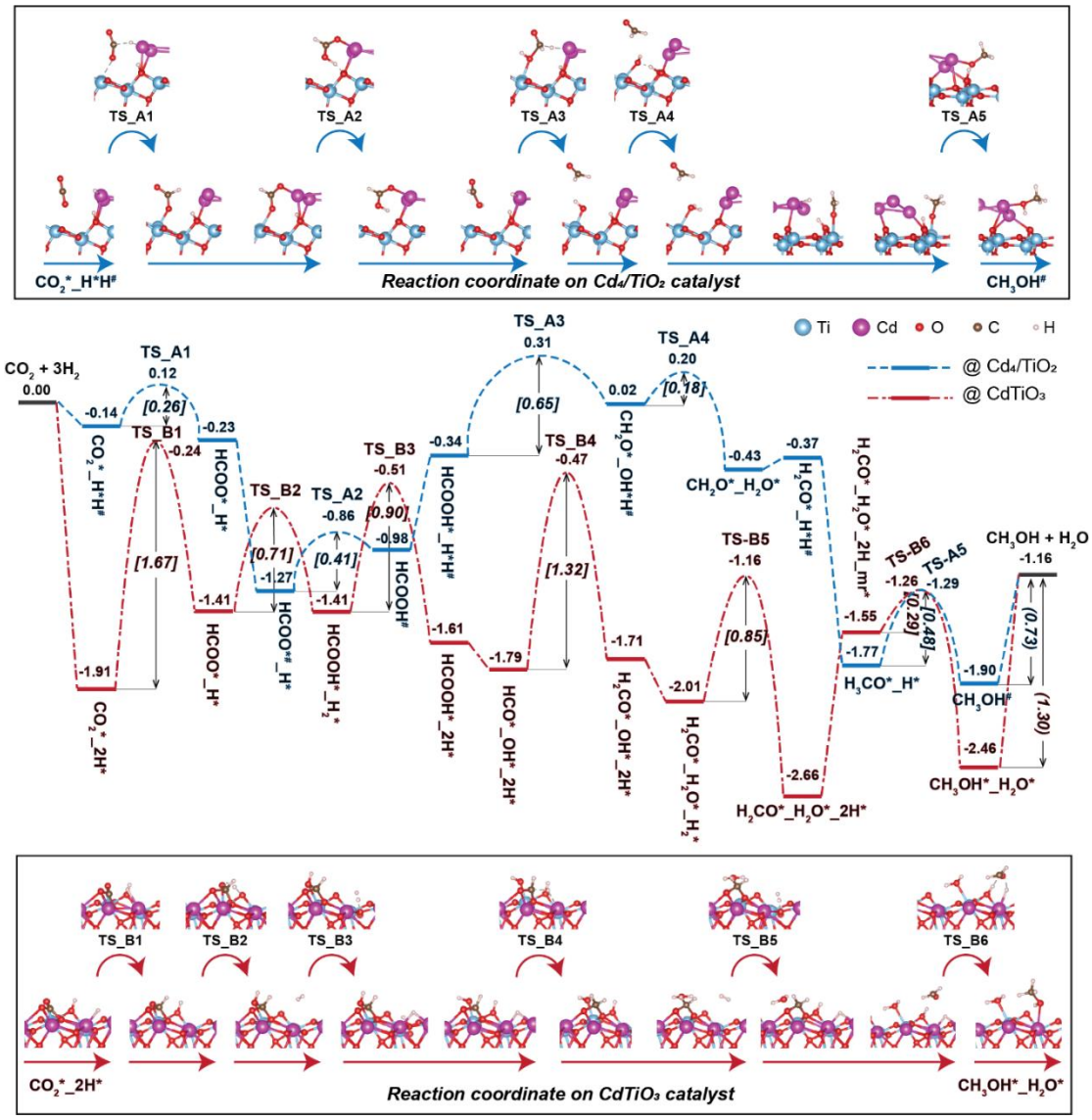

Fig 4. DFT calculations. Reaction energy profiles of CO_2 hydrogenation to CH_3OH on the Cd_4/TiO_2 and $CdTiO_3$ catalysts via the formate pathway. (unit: eV). For Cd_4/TiO_2 catalyst, the species with an asterisk (*) and hash sign ($^{\#}$) are species that interact with the TiO_2 site and Cd site of the Cd_4/TiO_2 catalyst, respectively.

The mechanism of the catalytic reactions over isolated Cd site and Cd cluster supported on TiO_2 were further studied by periodic DFT calculations. The computations indicate that the isolated Cd site has very low stability on both defect-free and O_v-containing TiO_2 surfaces (Fig. S10). Moreover, the $CdTiO_3$ phase is identified in the experiment as one of the components in the synthesized catalyst. Therefore, $CdTiO_3$ was chosen as an alternative potential active phase representing an isolated Cd site on the surface of TiO_2 (Fig. S11). The Cd_4/TiO_2 structure was optimized as a model for the Cd cluster site. The reaction pathways of CO_2 hydrogenation to CH_3OH via a formate mechanism over Cd_4/TiO_2 and $CdTiO_3$ catalysts are summarized in Fig. 4. For both surface models, the reaction starts with the heterolytic dissociation of an H_2 molecule with an activation energy of 0.39 and 0.92 eV for Cd_4/TiO_2 and $CdTiO_3$ catalysts, respectively. In the case of the Cd_4/TiO_2 model, the subsequent CO_2 hydrogenation takes place on the interface sites. The formation of H_2CO* intermediate is identified in this case as the most difficult step with the activation energy of 0.65 eV. An alternative mixed-oxide ($CdTiO_3$) is found to be much less reactive. The reaction path features two highly activated steps, namely, the initial

step of the CO_2 reduction and HCOO* formation (E_{act} = 1.67 eV) and HCO* reduction to H_2CO* (E_{act} = 1.32 eV). In general, the key reaction intermediates of HCOO*, HCOOH*, and CH_2O*_H_2O* on the surface of $CdTiO_3$ are much more stable compared to the respective states on the Cd_4/TiO_2 interface. Accordingly, the evolution of these intermediates along with the catalytic reaction coordinate proceeds with much higher barriers, evidencing a much higher catalytic CO_2 hydrogenation activity of the Cd_4/TiO_2 over the bulk $CdTiO_3$ mixed oxide phase.

4. Conclusions

In summary, this work reports a new Cd/TiO_2 catalyst that exhibits excellent performance for CO_2 hydrogenation to methanol. The metal-oxide interface containing the Cd and surface O-Ti moiety affords a synergetic reaction center for CO_2 conversion to methanol. The Cd cluster interacted with TiO_2 exhibits unique electronic properity, and is demonstrated more possible to be active site for CO_2 hydrogenation to methanol than nanometre-size Cd particle or isolated Cd site. The formation of H_2CO* intermediate is identified as the rate-determining step for CO_2 hydrogenation to methanol. The rate-determining step activation energy on the Cd cluster model is only half of that on isolated Cd site model.

Conflicts of interest

There are no conflicts to declare.

Author contributions

Prof. Can Li proposed the project, supervised the research, and revised the manuscript. Prof. Evgeny A. Pidko and Dr. Guanna Li supervised the DFT calculation and revised the manuscript. Jijie Wang and Zhe Han did experiments and wrote the manuscript. Jittima Meeprasert performed the DFT calculations and drafted part of the manuscript. Huan Wang did the catalyst evaluation. Zhendong Feng did the IR experiment. Chizhou Tang, Feng Sha, and Shan Tang analysis on some experimental and calculation results. All the authors participated in the discussion and agreed the conclusions of the manuscript.

Acknowledgments

We thank Prof. M. Chen (Xiamen University) for the help with the XPS experiments, Prof. R. Si (Sun Yat-sen University) and Dr. J. Zhang (DICP) for the help with the EXAFS experiments and data analysis. **Funding:** This work was supported by grants from National Key R&D Program of China (2017YFB0702800), National Natural Science Foundation of China (No. 21802139), Youth Innovation Promotion Association CAS (No. 2019183). E.A.P. thanks the European Research Council (ERC) under the European Union's Horizon 2020 research and innovation programme (grant agreement No. 725686). J. M. acknowledges

financial support through the Royal Thai Government Scholarship. DFT calculations were carried out using national computer facilities subsidized by the Netherlands Organization for Scientific Research (NWO) Domain Science.

Electronic supporting information

Supporting information is available in the online version of this article.

References

1. A. Goeppert, M. Czaun, J. P. Jones, G. K. Surya Prakash and G. A. Olah, *Chem. Soc. Rev.*, **2014**, 43, 7995–8048.
2. C. Shih, T. Zhang, J. Li, C. Bai, *Joule*, **2018**, 2, (10), 1925-1949.
3. X. Jiang, X. Nie, X. Guo, C. Song, J. Chen, *Chem. Rev.*, **2020**, 120, (15), 7984–8034.
4. J. Zhong, X. Yang, Z. Wu, B. Liang, Y. Huang, T. Zhang, *Chem. Soc. Rev.*, **2020**, 49, 1385-1413.
5. A. Alvarez, A. Bansode, A. Urakawa, A. V. Bavykina, T. A. Wezendonk, M. Makkee, J. Gascon, F. Kapteijn, *Chem. Rev.*, **2017**, 117, 9804−9838.
6. M. Porosoff, B. Yan, J. Chen, *Energy Environ. Sci.* **2016**, 9, 62–73.
7. G. Centi, S. Perathoner, *Catal. Today*, **2009,** 148, 191–205.

8. J. Graciani, K. Mudiyanselage, F. Xu, A. Baber, J. Evans, S. Senanayake, D. Stacchiola, P. Liu, J. Hrbek, J. F. Sanz, J. Rodriguez, *Science*, **2014**, 345, 546–550.
9. M. Behrens, F. Studt, I. Kasatkin, S. Kuhl, M. Havecker, F. A. Pedersen, S. Zander, F. Girgsdies, P. Kurr, B. L. Kniep, M. Tovar, R. W. Fischer, J. K. Norskov, R. Schlogl, *Science*, **2012**, 336, 893–897.
10. S. Kuld, M. Thorhauge, H. Falsig, C. F. Elkjær, S. Helveg, I. Chorkendorff, J. Sehested, Quantifying the promotion of Cu catalysts by ZnO for methanol synthesis. *Science*, **352,** 969–974 (2016).
11. S. Kattel, P. J. Ramirez, J. G. Chen, J. A. Rodriguez, P. Liu, *Science*, **2017**, 355, 1296–1299.
12. K. Larmier, W. C. Liao, S. Tada, E. Lam, R. Verel, A. Bansode, A. Urakawa, A. C. Vives, C. Coperet, *Angew. Chem. Int. Ed.*, **2017**, 56, 2318 –2323.
13. S. Kattel, B. Yan, Y. Yang, J. G. Chen, P. Liu, *J. Am. Chem. Soc.*, **2016**, 138, 12440−12450.
14. S. A. Kondrat, P. J. Smith, P. P. Wells, P. A. Chater, J. H. Carter, D. J. Morgan, E. M. Fiordaliso, J. B. Wagner, T. E. Davies, L. Lu, J. K. Bartley, S. H. Taylor, M. S. Spencer, C. J. Kiely, G. J. Kelly, C. W. Park, M. J. Rosseinsky, G. J. Hutchings, *Nature*, **2016**, 531, 83–87.
15. X. Dong, F. Li, N. Zhao, Y. Tan, J. Wang, F. Xiao, *Chin. J. Catal.*, **2017**, 38, 4, 717–725.

16. O. Martin, A. J. Martin, C. Mondelli, S. Mitchell, T. F. Segawa, R. Hauert, C. Drouilly, D. C. Ferr, J. P. Ramrez, *Angew. Chem. Int. Ed.*, **2016**, 55, 1–6.

17. G. Prieto, J. Zecevic, H. Friedrich, K. P. de Jong, P. E.de Jongh, *Nat. Mater*., **2013**, 12, 34–39.

18. F. Sha, Z. Han, S. Tang, J. Wang, C. Li, *ChemSusChem*, **2020**, 13, 6160–6181.

19. C. Li, G. Melaet, W. T. Ralston, K. An, C. Brooks, Y. Ye, Y. Liu, J. Zhu, J. Guo, S. Alayoglu, G. A. Somorjai, *Nat. Commun.*, **2015**, 6: 6538.

20. L. Wang, E. Guan, Y. Wang, L. Wang, Z. Gong, Y. Cui, X. Meng, B. C. Gates, F. Xiao, *Nat. Commun.*, **2020**, 11: 1033.

22. J. Ye, C. Liu, D. Mei, Q. Ge, *ACS Catal.*, **2013**, 3, 1296−1306.

21. J. Hu, L. Yu, J. Deng, Y. Wang, K. Cheng, C. Ma, Q. Zhang, W. Wen, S. Yu, Y. Pan, J. Yang, H. Ma, F. Qi, Y. Wang, Y. Zheng, M. Chen, R. Huang, S. Zhang, Z. Zhao, J. Mao, X. Meng, Q. Ji, G. Hou, X. Han, X. Bao, Y. Wang, D. Deng, *Nat. Catal.*, **2021**, 4, 242–250.

23. Z. Han, C. Tang, J. Wang, L. Li, C. Li, *J. Catal.*, **2021**, 394, 236–244.

24. S. Dang, B. Qin, Y. Yang, H. Wang, J. Cai, Y. Han, S. Li, P. Gao, Y. Sun. *Sci. Adv.*, **2020**, 6: eaaz2060.

25. J. Wang, G. Li, Z. Li, C. Tang, Z. Feng, H. An, T. Liu, H. Liu, C. Li, *Sci. Adv.*, **2017**, 3: e1701290.

26. J. Wang, C. Tang, G. Li, Z. Han, Z. Li, H. Liu, F. Cheng, C. Li, *ACS Catal.*, **2019**, 9, 10253-10259.

27. F. Studt, I. Sharafutdinov, F. A. Pedersen, C. F. Elkjar, J. S. Hummelshoj, S. Dahl, I. Chorkendorff, *Nat. Chem.*, **2014**, 6, 320–324.

28. E. M. Fiordaliso, I. Sharafutdinov, H. W. P. Carvalho, J. D. Grunwaldt, T. W. Hansen, I. Chorkendorff, J. B. Wagner, C. D. Damsgaard, *ACS Catal.*, **2015**, 5, 5827−5836.

29. B. V. Crist. Handbook of Monochromatic XPS Spectra: The Elements of Native Oxides, wiley, **2000**, ISBN: 978-0-471-49265-8.

30. S. Hejazi, S. Mohajernia, B. Osuagwu, G. Zoppellaro, P. Andryskova, O. Tomanec, S. Kment, R. Zboril, P. SchmukiI, *Adv. Mater.* **2020,** 1908505.

31. I. A. Fisher, A. T. Bell, *J. Catal.*, **1997**, 172, 222–237.